Numerical investigations of lightning phenomena

By J.-F. Ripoll†, C. Jeffery†, J. Zinn† AND P. Colestock†

We develop a numerical model of the lightning return stroke initiated by a vertical electrical field. Our model solves the Euler system and radiation transport in cylindrical geometry. We first validate the radiation hydrodynamics. We then derive the set of electrodynamic equations that simulate the initiation and growth of the discharge. For certain parameter configurations, we show that our lightning discharge simulations are consistent with observations. We also study the optical signature of the simulated lightning return stroke and demonstrate that these signatures depend greatly on the total energy input.

1. Motivation and objectives

Non-proliferation remote sensing is presently hindered by lightning events that trigger space-based electromagnetic pulse sensors. An additional characterization of the signal can then be obtained by synchronous optical measurements and helps to discriminate coincident events. However, the interpretation of the signal requires an understanding of the fundamental physics of lightning channel initiation, growth, and decay. Unfortunately this knowledge is currently lacking. Moreover, the space observations provide little insight into the nature, duration and strength of the lightning optical source because of the multiple-scattering in clouds, which smears out the lightning signal to a great extent. Numerical simulations are used here in order to better understand the signature and the evolution of the lightning return stroke channel.

The lightning return stroke is a shock of hot air produced by the electric discharge of a lightning event when it touches the ground. It involves a complex mix of compressible hydrodynamics and electrodynamics, chemistry, plasma physics, and radiative transfer that is not widely understood (Lowke 2004; Cooray 2003). This phenomena has been studied in the past, for instance in Plooster (1971), Paxton et al. (1986), and is not reviewed here (see, for instance, Cooray (2003); Lowke (2004)). The lightning return stroke model we have developed is fully described by Zinn et al. (2006), where other numerical experiments are also conducted. The shock propagation and its radiation have also been studied in Ripoll et al. (2006).

In this paper, we will first show through 23 computations that our code produces results that agree with self-similar profiles derived theoretically for cylindrical blast waves (Zel'dovich & Raizer 2002; Mihalas & Mihalas 1999). We also compare our shock-capturing scheme with a more accurate predictor-corrector scheme (Loubere 2004; Loubere & Shashkov 2005) in order to verify the accuracy of our shock propagation. These results validate our code. We then show results from three distinct types of model computations.

(1) In the first computation, we model the lightning stroke simply as a narrow cylindrical volume of impulsively heated air surrounded by a much larger volume of cold air. It is assumed that the heating is produced by the addition, at time zero, of a specified

† Los Alamos National Laboratory, ISR-2

amount of energy per unit length. We then compute the radiative hydrodynamics and chemical evolution of the system, including the evolving radial profiles of temperature, density, and chemical composition, and also the rate of output of visible light.

(2) In the second type of model we attempt to approximate the electrodynamic evolution of the discharge with the assumption that the discharge is initiated by the impulsive application of an intense axial electric field. The electric field is assumed to be derived from a charge on a hypothetical capacitance with a prescribed radius, with the approximation that the electric field direction is entirely axial. When the initial E field is above the Townsend discharge threshold it accelerates the ambient electrons to an extent such that the associated collisional ionization rate exceeds the sum of the electron-neutral attachment rate and the electron-ion recombination rate, so that the electron concentrations increase exponentially. As a result the axial electric current density increases exponentially, and with it so does the rate of ohmic energy input to the air. According to the well-known swarm experiment results described in numerous papers by A.V. Phelps et al. (Frost & Phelps 1962; Chanin *et al.* 1962; Engelhardt & Phelps 1963; Engelhardt *et al.* 1964; Hake & Phelps 1967), the effective electron temperatures and drift velocities depend almost entirely on the ratio of the applied electric field and the background atom/molecule/ion density, and so do the collisional electron/ion production rates and the electron-neutral attachment rates. Using fits of the Phelps et al. data, we compute the evolving electron temperatures, drift velocities and rate coefficients and the evolving electron concentrations and air chemical composition. From these we then compute the electrical conductivities and current densities, as well as the rates of ohmic energy input to the gas and the rate of discharge of the applied charge on the hypothetical capacitor. The computed electron concentrations and plasma energy densities and electric currents rise then very rapidly until the charge on the capacitor is drained to a point where the associated axial E field drops below the Townsend threshold and the discharge quenches. In the process, a definite amount of energy is delivered to the discharge channel. During this discharge period, and for some time afterward, we compute the rates of hydrodynamic expansion and radiative transport and the changes in chemical composition. During the later phase the computation is similar to the type 1 model described previously, and the results can be compared. We find, however, with the above discharge model that the electric currents tend to rise rapidly to very large values, such that a very large electromagnetic pulse would be produced, and in the course of which the inductive electric fields in the current channel and surroundings would be quite large and would moderate the net E field and the rate of current buildup in the channel. The associated very large magnetic fields would exert simultaneously a substantial radial pinching force on the channel plasma. Thus for a realistic model we would have to treat all of these processes self-consistently.

(3) In order to proceed, but without attempting to do a full numerical integration of Maxwell′s equations for the radiating electromagnetic pulse, we have developed a third model: we approximate the induced E field effects associated with the radiating electromagnetic wave by means of an assumed self-inductance L per unit length. We compute then the rate of rise of the radially integrated electric current, $\partial I/\partial t$, and the induced E field as $-L\partial I/\partial t$. This leads however to numerical integration problems that we have not yet fully solved. We nevertheless present some preliminary numerical results where we have assumed a value of the inductance L some 100 times smaller than the expected actual value. We will show that they are overall in the range of observational data. Finally, in Section 3.3 we derive an alternative set of equations that may represent the

evolution of the induced electric field better than the ones involving our approximate self-inductance model described previously. These may avoid some of the problems we encountered, but they have not yet been incorporated into the full-scale numerical model.

2. Code validation

2.1. *Comparison with blast wave theory*

As the lighting channel expands, a cylindrical shock develops that radiates outward at supersonic velocities. The shock position, $R_n(t)$, is associated with a pronounced density maximum that is a product of the velocity divergence created as the hot air expands into the still background air. Since the speed of sound in air increases with temperature, the hot air behind the shock accelerates forward to maintain a sharp discontinuity while geometric attenuation acts to mitigate the front. When these processes are in balance, as self-similar shock profile develops that can be derived from the continuity, mass and energy equations. The derivation of self-similar shock profiles assumes a discontinuity; the resulting solutions are therefore weak solutions of the hydrodynamic equations.

The self-similar shock solution gives $\rho = 0$ at $r = 0$ without radiation; this density minimum is associated with a divergent temperature. As a result, the self-similar solutions are only expected to be valid in the vicinity of the shock. Straightforward dimensional analysis for the shock position, R_n, and the shock velocity, W_n, using the initial input channel energy density E_0 (J/m) and mass density ρ_0 yields

$$R_n \sim (E_0/\rho_0)^{1/4}\, t^{1/2} \quad \text{and} \quad W_n \sim (E_0/\rho_0)^{1/4}\, t^{-1/2}.$$

These expressions are derived in the case where no radiation is included in the equations and will describe roughly radiation effects on the shock according to Mihalas & Mihalas (1999). However, they should provide an approximate behavior of the shock for a certain range of parameters and time. We validate our shock-capturing numerical scheme—the Von Neumann-Richtmeyer scheme (Richtmeyer & Morton 1967; Zinn 1973), —by verifying these scaling relations. The results of 23 radiation-hydrodynamic simulations performed for temperature $T \in \{1.03 \times 10^4, 3.61 \times 10^4, 1.01 \times 10^5, 4.0 \times 10^5, 8.46 \times 10^5\}$ K and initial radius $r_0 \in \{0.1, 0.3, 1, 3, 10\}$ cm are shown in Fig. 1. Figure 1(a) shows R_n, while 1(b) shows R_n normalized by $(E_0/\rho_0)^{1/4}$. For low initial temperatures and small initial radii, self-similar behavior is observed for a relatively short period near $t = 100$ microseconds. However, for high initial temperatures and large initial radii, the $t^{1/2}$ scaling is observed until $t = 10$ milliseconds. These results provide an additional validation of our numerical code and also indicate the importance of shock physics in determining the evolution of the lightning return stroke channel. The results of Fig. 1 are reiterated in Fig. 2, which shows the velocity as a function of time, both unnormalized 2(a) and normalized 2(b). Figure 2(b) highlights the importance of large initial temperature in the formation of a self-similar shock profile with $W_n \sim t^{-1/2}$ behavior persisting until 10 milliseconds for the hottest simulations.

2.2. *Comparison with a second hydrodynamic code*

A cylindrical shock of air at an altitude of 8 km ($\rho = 5.41 \times 10^{-4}$ g/cc) initiated by a 1 cm discontinuity of energy of $E_l = 1.61 \times 10^{12}$ and $E_r = 1.6 \times 10^9$ Erg/g is considered. The solution of our hydrodynamics solver (denoted LS) is compared to a reference solution obtained by a Lagrangian predictor-corrector scheme (Loubere 2004; Loubere & Shashkov 2005) (denoted PC). Our goal is to define the best spatial resolution and viscous pressure

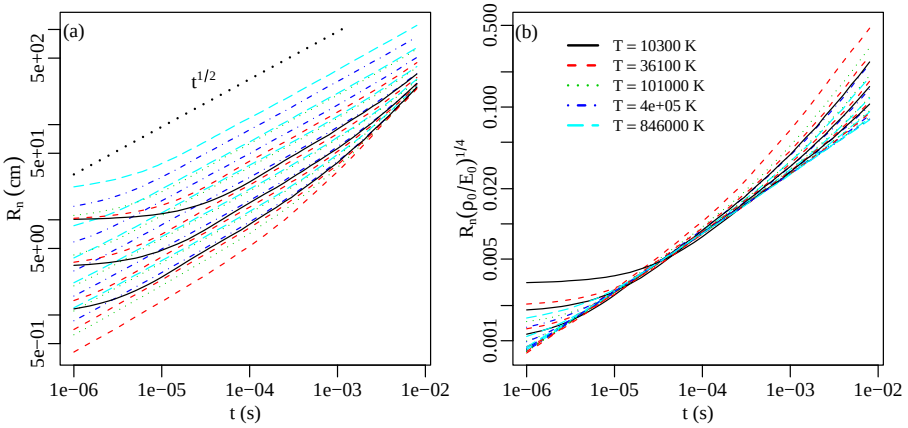

FIGURE 1. Evolution of the shock position R_n; (a) in cm, (b) normalized by $(E_0/\rho_0)^{1/4}$.

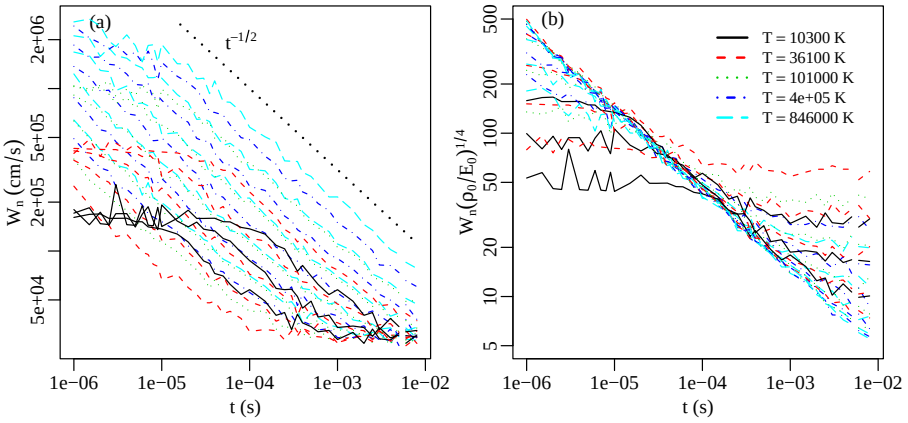

FIGURE 2. Evolution of the shock velocity W_n; (a) in cm/s, (b) normalized by $(E_0/\rho_0)^{1/4}$.

coefficients such that the shock is relatively well resolved (in terms of position, amplitude, and spatial diffusion) for the smallest number of nodes. The computation is made with a variable γ in the lightning case, accounting for the air composition, while the reference solution has been obtained using the perfect gas law with $\gamma = 1.2$. The reference solution is sharply resolved with 170 000 nodes. Results are shown in Fig. 3. Only 360 nodes were used in our computation and the accuracy of our results is considered satisfactory.

3. Computation of the current growth in the channel

3.1. *Equations and numerical schemes*

The current discharge is assumed to be produced by a 1-D capacitor model that vertically discharges a prescribed amount of energy in the initially prescribed 1 cm channel. The current, the fields, and the chemistry introduce source terms in the Euler system that are implicitly discretized to avoid time steps that are too small because of the stability CFL condition.

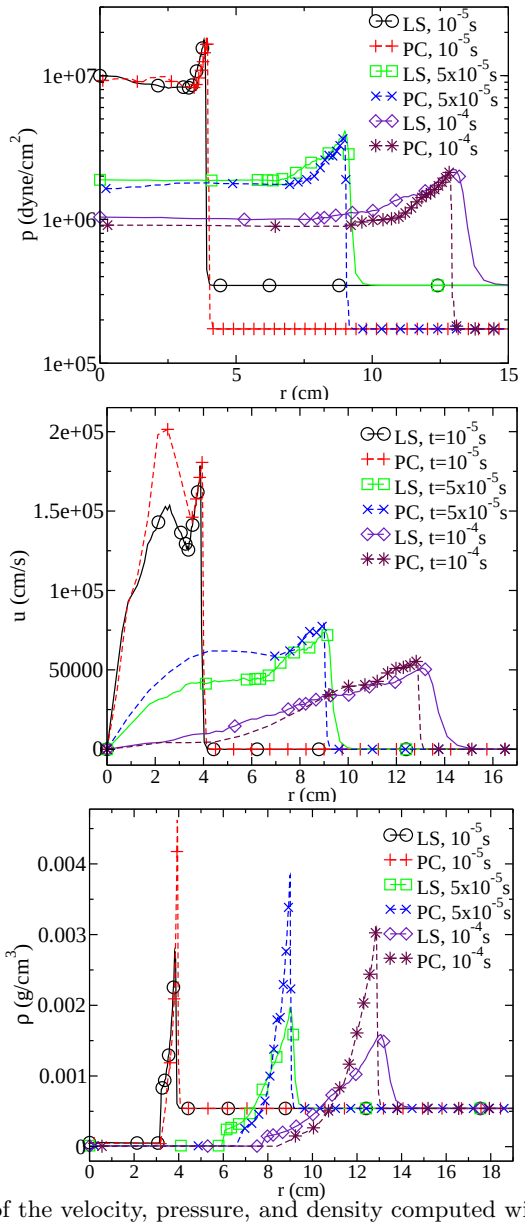

FIGURE 3. Evolution of the velocity, pressure, and density computed with two different codes.

Let us first assume that the hydrodynamic quantities (density ρ^n, gas velocity v^n, temperature T^n, pressure p^n), the concentrations of our 687 species describing the air plasma, and the electric quantities (temperature of electrons T_e^n, electric field E^n, current discharge I^n, charge Q^n, and capacitance C^n) are all known at t^n. We now evaluate implicitly the chemistry and the electrical quantities as follows. The evolution of the electron concentration is given by

$$\frac{\partial n_e}{\partial t} = \sum_i P_i - D_i = n_e[K_i(O_2, N_2, ...) - K_a(O_2, ...) - K_r(O^+, N^+, O_2^+, N_2^+, ...)].$$

where K_i, K_a, K_r respectively accounts for the ionization, attachment, and recombination processes of all species. This equation provides n_e^{n+1}, which has been solved implicitly with the other species. However, the explicit electron temperature T_e^n and the explicit hydrodynamic states at t^n have been used. The electric current density J is given by the conductivity equation $J = \sigma E$ discretized as follows:

$$J^{n+1} \simeq \sigma^{n+1} E^n = |e| n_e^{n+1} v_e^n E^n. \tag{3.1}$$

where σ is the conductivity and E the z-component of the electric field. v_e is the electron drift velocity and e is the electron charge. We have assumed $v_e^{n+1} \simeq v_e^n = v_e(E^n, {n_n}^n)$. v_e is obtained through the Phelps tables (Frost & Phelps 1962; Chanin *et al.* 1962; Engelhardt & Phelps 1963; Engelhardt *et al.* 1964; Hake & Phelps 1967), which have been interpolated in Eq. (3.7). As a first approximation, the neutral particle density n_n is obtained from the density of the cold air and is hence constant in time (see also Section 3.2). The variation of current at t^{n+1} is thus only related to the variation of the electron concentration at t^{n+1}. Given J^{n+1}, we obtain I^{n+1} using

$$I(r) = \int_0^R 2\pi r J(r) dr. \tag{3.2}$$

We also compute the first-order time derivative of the current $\partial_t I_{|n+1/2} = (I^{n+1} - I^n)/\Delta t$. The induced electric field, $E'_{|n+1/2}$, is then obtained from

$$E'_{|n+1/2} = -L_{eff}^n \frac{\partial I}{\partial t}_{|n+1/2}, \tag{3.3}$$

where $L_{eff}^n = 10^{-2} L^n$ with L^n assumed to be the inductance of a straight wire of length $l = 10\,\mathrm{m}$ at t^n, given by : $L^n(r) = 1.112 \times 10^{-12} max(2 \times 10^9 (log(2l/r^n) - 0.75), 0)$. (This expression comes from the *Handbook of Chemistry and Physics (1962)*). As noted in Section 1, we encountered serious numerical problems when we attempted to use this expression for the inductance. As a temporary measure we have used an artificially reduced value of L equal to .01 times that value. From the current I^{n+1}, we can also deduce the magnetic field B^{n+1} by discretizing the Maxwell-Faraday law $\nabla \times B = 4\pi/c\, J$, which leads to

$$B^{n+1}(r) = \frac{2}{c\, r} I^{n+1}(r). \tag{3.4}$$

The evolution of the charge Q is given by

$$\frac{\partial Q}{\partial t} = -\Delta I^{n+1}. \tag{3.5}$$

It gives Q^{n+1} knowing I^{n+1} through the relationship $Q_i^{n+1} = Q_i^n - \Delta_i I_i^{n+1} \Delta t = Q_i^n - A_i J_i^{n+1} \Delta t$ with $A_i = \pi(r_{i+1}^2 - r_i^2)$ for all nodes i. From the electrostatic and induced electric field, the new total electric field is deduced by

$$E^{n+1} = \frac{Q^{n+1}}{C^{n+1}} + E'_{|n+1} \simeq \frac{Q^{n+1}}{C^n} + E'_{|n+1/2}. \tag{3.6}$$

The capacitance C^n of our capacitor evolves as the initial channel expands following $C^n = C^0 (r^n / r_{max})^2$ with r_{max} is the maximum channel radius. C^0 is chosen such that the resulting initial electric field of a charge $Q^0 = 2\,C$ is $E^0 = 1\,\mathrm{kV/cm}$. The interpolated Phelps' tables give T_e and v_e according to

$$T_e = 1.318 \times 10^{15} (\frac{E}{n_n})^{.61} \quad \text{and} \quad V_e = -2.20 \times 10^{15} (\frac{E}{n_n})^{.65} \frac{1}{E}. \tag{3.7}$$

where n_n is assumed to be given by the cold air at density ρ_0 by $n_n = 2.09 \times 10^{22}\rho_0$.

The chemistry and electric quantities have now been computed at t^{n+1}. The algorithm works as follows. From Eq. (3.1) and Eq. (3.4), we obtain the $J^{n+1} \times B^{n+1}$ term, which describes electromagnetic effects in the momentum equation of the Euler equations. From Eq. (3.2) and Eq. (3.6), the ohmic heating term $E^{n+1}I^{n+1}$ is included in the energy equation of the Euler system. Using the electron temperature and the species concentrations at t^{n+1}, a correction is made to the opacity value, which is initially only obtained from the hydrodynamic state, through tables. The radiation contribution is then computed and included in the energy equation. Our Euler system, including ohmic, magnetic, and radiative effects can now be solved. It produces the new hydrodynamics quantities ρ^{n+1}, v^{n+1}, T^{n+1}, p^{n+1} at t^{n+1}. The full system is thus closed.

3.2. *Chemical equilibrium assumption*

Our chemistry is defined for non-equilibrium air at low temperatures, below 8 000 K. We arbitrarily extend its range of application to 30 000 K. At this temperature, air is hot enough to be fully ionized. Collisions are then so fast that chemical equilibrium can be assumed. The chemistry is thus described by equilibrium state laws. At equilibrium, $T_e = T$ and $n_e = n_i$, with n_i the number of ions. The total number N_{total} of neutrals, ions, and electrons is given through the state law $N_{total} = p/kT$. The number of neutrals n_n is then obtained from the density ρ and from its mass m. We have $n_n = \rho/\bar{m}$, where $\bar{m}$ is the average atomic mass of air at equilibrium, $\bar{m} = 2.406 \times 10^{-23}$ g. It comes from the known composition of dissociated and ionized air (78% of N, 21% O, etc.). The number of electrons at equilibrium is thus deduced from $n_e = N_{total} - n_n = p/kT - \rho/\bar{m}$ and is not solved from Eq. (3.1).

3.3. *Alternative equation set for describing the electric discharge*

We first consider a cylindrical channel that carries an axial current and assume that the field is quasi-static. Maxwell's equations are given by

$$\nabla \times \mathbf{B} = \frac{4\pi}{c}\mathbf{J} + \frac{1}{c}\frac{\partial \mathbf{E}_{tot}}{\partial t}, \tag{3.8}$$

$$\nabla \times \mathbf{E}_{tot} = -\frac{1}{c}\frac{\partial \mathbf{B}}{\partial t}, \tag{3.9}$$

where $\mathbf{J} = \sigma \mathbf{E}_{tot}$. The total electric field $\mathbf{E}_{tot}$ is defined by $\mathbf{E}_{tot} = \mathbf{E}_S - \mathbf{E}_{ind}$, where $\mathbf{E}_S$ is the electrostatic field due to the charge separation in the thundercloud. $\mathbf{E}_S$ is assumed to be given by the charge and the capacitance of a hypothetical capacitor. We write $\mathbf{E}_S = Q/C\hat{\mathbf{z}}$, which is initially pointing downward. In such a referential, $\mathbf{E}_{ind}$ is pointing upward, which explains the sign difference. Later, when the current decreases, $\mathbf{E}_{ind}$ could point downward. By definition, the electrostatic field comes from a potential and can always be written as $\mathbf{E}_S = \nabla\phi$. We denote $\mathbf{E} = \mathbf{E}_{tot}$ and the full wave equation is given by

$$\nabla \times \nabla \times \mathbf{E} + \frac{4\pi}{c^2}\frac{\partial \mathbf{J}}{\partial t} + \frac{1}{c}\frac{\partial^2 \mathbf{E}}{\partial t^2} = 0. \tag{3.10}$$

Taking the quasi-static approximation on Eq. (3.10) leads to

$$\nabla \times \nabla \times \mathbf{E} + \frac{4\pi}{c^2}\frac{\partial \mathbf{J}}{\partial t} = 0. \tag{3.11}$$

In 1-D cylindrical coordinates and using the conductivity equation, it gives

$$\frac{\partial(\sigma E_z)}{\partial t} - \frac{c^2}{4\pi}\frac{1}{r}\frac{\partial}{\partial r}\left(r\frac{\partial E_z}{\partial r}\right) = 0. \tag{3.12}$$

The boundary conditions $E^z_{tot}(z = 0) = Q(r_0)/C(r_0)$. As in Section 3.1, the charge Q obeys Eq. (3.5). C is computed as previously.

4. Numerical simulations

Three types of simulations have been performed:

1- Computations in which only a radiating hydrodynamic shock is initiated from an initial amount of energy (17 kJ/cm and 2.5 kJ/cm). Thus, no discharge, electron growth, or current are resolved.

2- Computations in which the initial electric field is given by the charge and capacitance of our capacitor model. The capacitor discharges its charge in time according to the model described in Section 3.1, but without including any induced electric and magnetic fields ($E_{ind} = 0$ in Eq. (3.6) and $B = 0$). We call this model the capacitor discharge (CD) model.

3- Computations in which the full lightning discharge model (denoted FM) described in Section 3.1 with capacitor, induced electric and magnetic fields has been used. This model works as follows. The initial electrostatic field is given by the charge and capacitance of the capacitor model. The energy is progressively released in the system through ohmic effects. As the number of electrons grows, the current and its gradient increase. This induces an opposing electric field (Eq. (3.3)) which decreases the total electric field. The effect of the induced electric field is thus crucial since it can limit the energy the capacitor releases in the system.

4.0.1. *General results and comparisons with observed data*

The goal is to characterize the current growth, the temperatures achieved, the amount of energy released by the discharge model, and the optical signature. At $t = 0$, the channel has an initial radius of 1 cm, which is covered by 8 cells. We plot quantities evolving in time for the 4th, 8th, 9th cells ($R_{4,8,9}$). We simulate a return stroke at 8 km, assuming an initial 2 Coulombs charge in the channel in a 1 kV/cm electric field. The charge value is common for lightning discharges, however the electric field is 10 times higher than the observed ones (Cooray 2003 p. 356). Such a value is taken in order to exceed the Townsend threshold value and create the discharge. This brings the total energy in the system of 2.5 kJ/cm in the full lightning discharge model and 17 kJ/cm in the capacitor model. The first value is realistic, the second is an order of magnitude too high, since the energy dissipated by a lightning event ranges between 1 and 10^3 J/cm (Cooray 2003 p. 210). In Fig. 4 (left), we compare the maximum temperature evolving in time of the lightning discharge computed with the capacitor model and with the full lightning discharge model. We observed that the maximum of heat released is higher and released 10 times faster (0.6 μs), when the induced electric field is absent of the model. This is due to the current, which is stronger and released faster when computed without induced electric field (Fig. 4 (right)). The peak current is approximately 100 kA in the full lightning discharge model, which is slightly too high (Fig. 4 (right)). Regular negative strokes have observed peak currents ranging between 14 to 80 kA and being approximately 30 kA in 50% of the case (Cooray 2003 p 166). We noticed, however, that our time average value of the current is realistically approximately 25 kA during

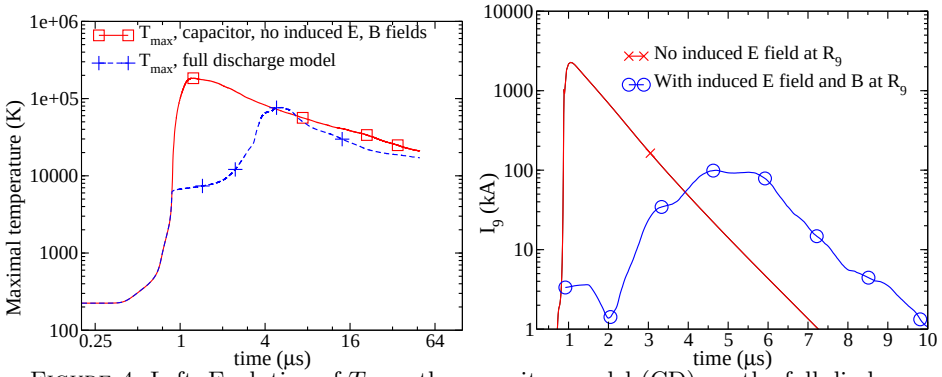

FIGURE 4. Left: Evolution of T_{max}; the capacitor model (CD) vs. the full discharge model (FM). Right: Evolution of the current (radius R_9) computed with the CD and FM models.

the 10 μs of the discharge. Additionally, the average value of the maximum temperature over 10 μs is approximately 31 000 K, while an average observed visible temperature is approximately 20 000 K, ranging between 15 000 and 30 000 K according to Cooray (2003) p. 164. Our results are coherent since the maximum temperature represents the temperature of the core of the lightning channel, which, we believe, remains opaque during a few microseconds and should have a higher temperature than those observed (see Section 4.0.2).

When using only the capacitor model, the peak current exceeds 2 MA (Fig. 4 (right)). This value is 10 times higher than the highest peak current observed in positive return strokes, which can reach $250-300$ kA (Cooray 2003 p. 166). This shows that accounting for the induced electric field is fundamental for predicting realistic values. Without it, the time averaged current is around 115 kA during the 10 μs of the discharge, which is too high by an order of magnitude. For the same reason, the time averaged maximum temperature of 70 000 K is also too high.

In Fig. 5 (left) we plot the electron density at two radii evolving in time and the current for the full lightning discharge model. The electron density is normalized by $N_{emax} = 2.8 \times 10^{19}$ cm^{-3}. According to Cooray (2003) p. 164, it ranges between 10^{17} and 10^{18} cm^{-3} in return strokes. Our peak values are then slightly too high, explaining the slightly too high peak current. In Fig. 5 (right), all fields are plotted evolving in time. They are normalized by $E_{max} = 1$ kV/cm and $B_{max} = 1.5$ Wb/m^2. The induced electric field decreases the total electric field. The capacitor is fully discharged in 10 μs and a maximum temperature of the channel core of 100 000 K is reached (Fig. 4 (left)). This temperature has been halved by the induced electric field. The latter drops the total electric field below the Townsend threshold value, which, in our case, is found around 0.97 kV/cm and is very close to the initial field. As a result, even though the induced electric field only represents 10% to 20% of the total electric field, its impact is significant. Furthermore, the magnetic field reduces the channel expansion. As a result, the heat is condensed in the core, which reaches a higher temperature than it would if B was not included. At a distance of one kilometer, we can calculate from B_{max} (occurring around 1 cm) that B would be around 1.5×10^{-5} Wb/m^2. This agrees with the observed range, between 10^{-6} and 10^{-5} Wb/m^2, and the 10^{-5} Wb/m^2 observed peak value (Cooray 2003 p. 171).

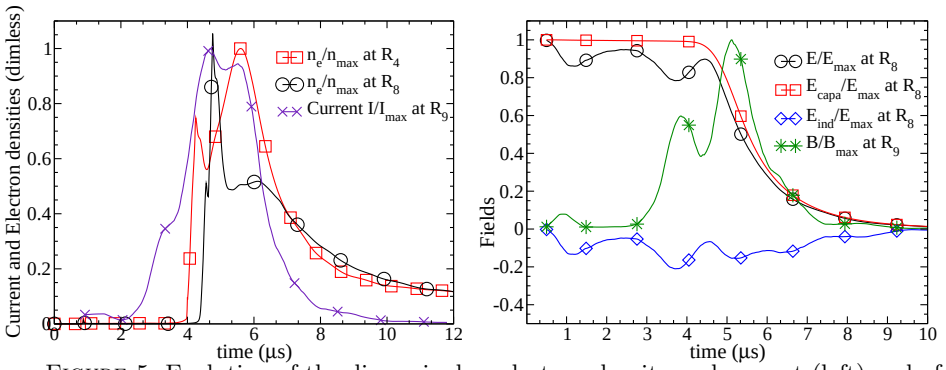

FIGURE 5. Evolution of the dimensionless electron density and current (left) and of the dimensionless electric and magnetic fields (right), computed with the full discharge model.

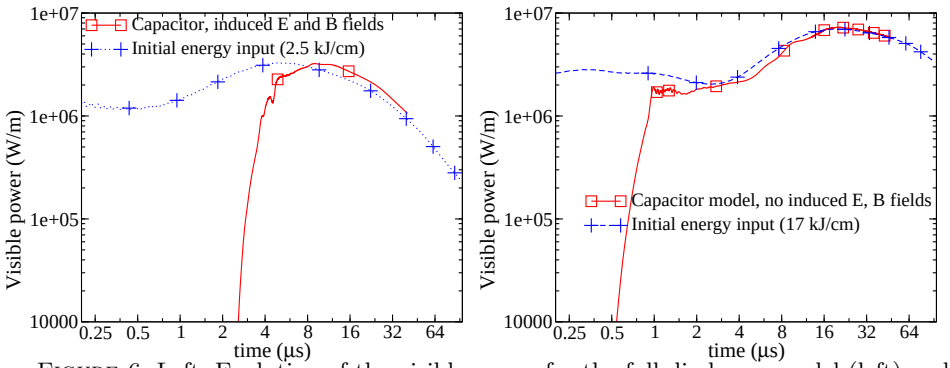

FIGURE 6. Left: Evolution of the visible power for the full discharge model (left) and the capacitor model (right) vs. a 2.5 kJ/cm and a 17 kJ/cm initial energy release.

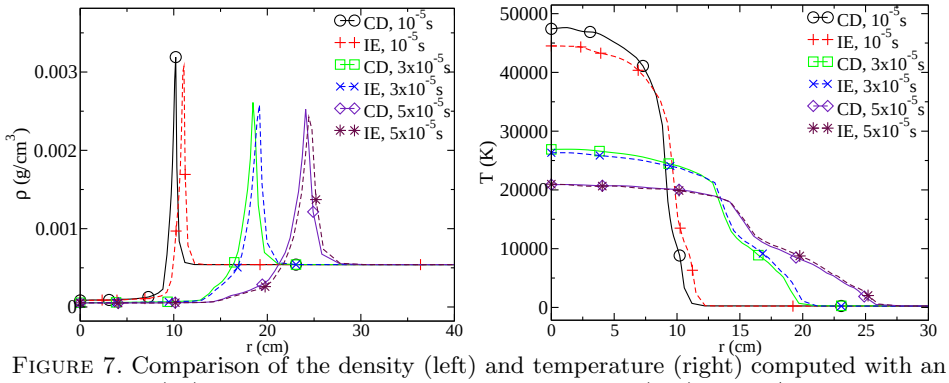

FIGURE 7. Comparison of the density (left) and temperature (right) computed with an initial energy input (EI) vs. using the capacitor discharge model (CD). 17 kJ/cm has been released.

4.0.2. *Optical signatures*

One goal of this study is to characterize the optical visible power of the lightning return stroke. In Cooray (2003) p. 162, the observed peak radiance ranges between 6×10^5 and 10^6 W/m, while the time and space averaged values of this quantity range between 0.7×10^5 and 2×10^6 W/m. We see in Fig. 6 (left) that our full discharge model realistically computes the optical power: we have a slightly too high peak value of 3.2×10^6 W/m, but our average in time over 10^{-2} s is around 1×10^5 W/m. The observed rise time is

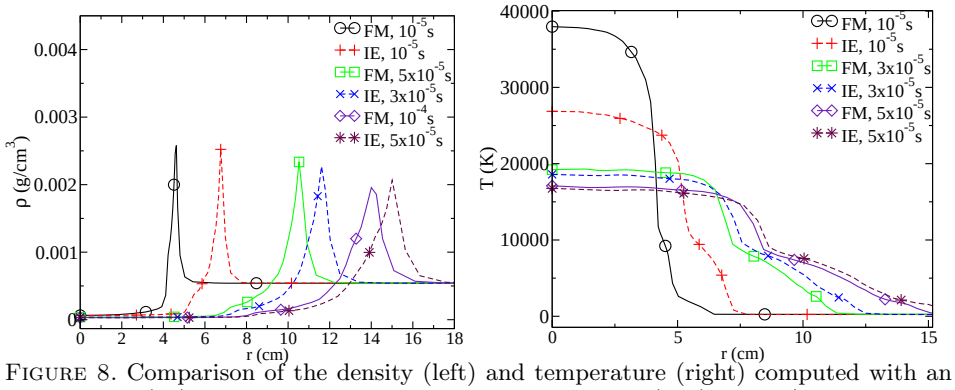

FIGURE 8. Comparison of the density (left) and temperature (right) computed with an initial energy input (EI) vs. using the full lightning discharge model (FM). 2.5 kJ/cm has been released.

between 1.5 and 4 μs for the common negative return stroke and can reach 10 μs for strong positive return stroke (Cooray 2003 p. 161). Thus, we see in Fig. 6 (left) that the computed rise time of 6 μs is quite realistic. Moreover, the time of the maximum corresponds to only double to triple the time of the equivalent minimum of 10^{-6} W/m. The capacitor model predicts a maximum value of 7.3×10^6 W/m, not in the observed range. It also takes 20 μs to reach the maximum visible power, which indicates that a very hot and opaque core channel lives during this time (cf. below). Moreover, the time of the maximum corresponds to 10 times more than the time of the minimum. The rise time is therefore also an important criteria for discriminating lightning events.

The evolution of the optical power is explained as follows: first, in a few microseconds or less (according to the model chosen), the full amount of energy is released by the discharge. The following increase of the optical power corresponds to the increase by expansion of the semi-transparent (to visible) emitting hot front, which precedes the hot and opaque channel core of the lightning. The visible power increase is due to the channel expansion, which is faster than the channel loss of energy (Zinn 1973). When the channel temperature has dropped enough (by expansion and radiation), such that the gas of the channel core becomes semi-transparent/transparent, the peak of visible emission is reached and the whole channel heat becomes visible. The decay of the visible power that follows is initially due to a fast loss of energy by radiation, since the whole channel is now more and more transparent radiating energy away, and then to adiabatic expansion.

The second goal of this study is to understand if the lightning optical signature can be predicted accurately without simulating the whole discharge process, which requires complex chemistry and plasma physics modeling. We prove in Fig. 6 that if an amount of energy, corresponding to the amount that the discharge produces, creates a shock wave that expands and radiates, then the resulting optical signature will be identical to the one of the discharge. This is true regardless of the discharge model used (Fig. 6). Figures 7 and 8 show that the temperature and density of both discharge models are also very close to those of the radiating shock of equivalent energy. They differ early on because the discharge model inputs the energy at a finite speed, but become similar after the full release of the charge. This happens before both the time of the maximum visible power and the time of the rise process (itself due to the hot channel expansion, as previously mentioned). In conclusion, the whole signature of the rise process is correctly described by the simple expanding radiating shock (Fig. 6).

5. Conclusions

Our numerical code and methods have been validated on simple hydrodynamics and radiation-hydrodynamics cases. We have presented our lightning discharge model and derived a second model in which the magnetic effects are consistent. We have shown some of our attempts to simulate the initiation of the lightning discharge. The numerical results for the full discharge model are in the range of observed data. This study also indicates that the optical signature of the lightning return stroke can be obtained from an expanding and radiating shock initiated by an equivalent amount of energy. The rise time of the visible power has been found to be a good criteria to discriminate lightning return stroke in addition to the maximum visible power of the return stroke.

Acknowledgments

With gratitude, we thank Dr. Loubere who provided the reference results used in Section 2.2. This work was funded by the Department of Energy / National Nuclear Security Agency.

REFERENCES

Borovsky, J. 1995 An electrodynamic description of lightning return strokes and dart leaders: Guided wave propagation along conducting cylindrical channels. *J. Geophy. Res.*, **100**(D2), 2697–2726.

Chanin, L.M., Phelps, A.V., Biondi, M.A. 1962 Measurements of the attachment of low-energy electrons to oxygen molecules. *Phys. Rev.*, **128**, 219–230.

Cooray, V. 2003 The lightning flash. The Institution of Electrical Engineers, London.

Engelhardt, A.G., Phelps, A.V. 1963 Elastic and inelastic collision cross sections in hydrogen and deuterium from transport coefficients. *Phys. Rev.*, **131**, 2115–2128.

Engelhardt, A.G., Phelps, A.V., Risk, C.G. 1964 Determination of momentum transfer and inelastic collision cross sections for electrons in nitrogen using transport coefficients. *Phys. Rev.*, **135**, A1566–A1574.

Frost, L.S., Phelps, A.V. 1962 Rotational excitation and momentum transfer cross sections for electrons in H_2 and N_2 from transport coefficients. *Phys. Rev.*, **127**, 1621–1633.

Hake, R.D., Phelps, A.V. 1967 Momentum-transfer and inelastic-collision cross sections for electrons in O_2, CO and CO_2. *Phys. Rev.*, **158**, 70–84.

Handbook of Chemistry and Physics 1962 Chemical Rubber Pub Co, 44th Ed. See also www.consultrsr.com/resources/eis/induct5.htm.

Loubere, R. 2004 First steps into ALE INC(ubator). A 2D arbitrary-Lagrangian-Eulerian Code on general polygonal mesh for compressible flows - Version 1.0.0. *Los Alamos Report LAUR 04-8840.*

Loubere, R., Shashkov, M. 2005 A subcell remapping method for polygonal staggered grids. *J. Comp. Phys.*, **209**, 105–138.

Lowke, J.J. 2004 On the physics of lightning. *IEEE Trans. on Plasma Sci.*, **32**, 4–17.

Mihalas, D., Mihalas, B. 1999 Foundations of radiation hydrodynamics. Dover.

Plooster, M. 1971 Numerical model of the return stroke of the lightning discharge. Phys. Fluids, **14**, 2124–2133.

Paxton, A.H., Gardner, R.L., and Baker, L. 1986 Lightning return stroke. A numerical calculation of the optical radiation. Phys. Fluids, **29**, 2736–2741.

Richtmeyer, R.D., Morton, K.W. 1967 Difference methods for initial-value problems. Interscience, New York.

Ripoll, J.-F., Jeffery, C., Zinn, J., Colestock, P. 2006 Modeling radiative transfer for the lightning return stroke channel. *Los Alamos report LAUR-05-9527.*

Zel'dovich, Ya.B., Raizer, Yu.P. 2002 Physics of shock waves and high-temperature hydrodynamic phenomena. Dover.

Zinn, J. 1973 A finite difference scheme for time-dependent spherical radiation hydrodynamics problems. *J. Comp. Phys.*, **13**, 569–590.

Zinn, J., Colestock, P., Jeffery, C., Ripoll, J.-F. 2006 Some numerical experiments related to lightning. To be submitted to *J. Geophys. Res.*